Cytokine 123 (2019) 154742

Contents lists available at ScienceDirect

Cytokine

journal homepage: www.elsevier.com/locate/cytokine

Adipokine zinc-α2-glycoprotein alleviates lipopolysaccharide-induced inflammatory responses through the β3-AR/PKA/CREB pathway

Jun Guo, Yanfei Li, Ruqian Zhao, Xiaojing Yang*

MOE Joint International Research Laboratory of Animal Health and Food Safety, Nanjing Agricultural University, Nanjing 210095, PR China

ARTICLE INFO

Keywords:
Zinc-α2-glycoprotein
Inflammation
Lipid metabolism
Mitochondria

ABSTRACT

Humans and animals frequently experience dysmetabolism induced by inflammation. Zinc-α2-glycoprotein (ZAG), a newly identified adipokine, is potentially involved in lipid metabolism. Our previous study revealed that the ZAG content increased after lipopolysaccharide (LPS) treatment. To clarify ZAG's possible effects on inflammatory responses and lipid metabolism, we used gene overexpression and knockout mice as models to investigate the function of ZAG during inflammation. The results showed that LPS increased plasma triglyceride, non-esterified fatty acid and hepatic triglyceride, while ZAG overexpression decreased these effects. Furthermore, ZAG overexpression weakened inflammatory responses, suppressed lipogenesis, and improved mitochondrial function during inflammation. ZAG overexpression also increased β3-adrenoreceptor, protein kinase A, and phosphorylated cyclic adenosine monophosphate-response element binding protein (CREB), promoted the combination of CREB and CREB-binding protein (CBP), and competitively inhibited the combination of nuclear factor-κB and CBP. After ZAG knockout, LPS-induced the hyperlipidemia worsened. ZAG knockout aggravated inflammatory responses, promoted lipogenesis, and weakened mitochondrial function during inflammation. ZAG knockout also decreased β3-adrenoreceptor and protein kinase A. The present study demonstrated that ZAG alleviated lipid metabolism disorders by weakening inflammatory responses. The β3-adrenoreceptor/protein kinase A/CREB pathway mediated the effects of ZAG on inflammation. These results will provide new insight for research on anti-inflammation.

1. Introduction

Humans and animals frequently experience inflammation [1,2]. During inflammation, the immune system is acutely activated and produces many inflammatory factors. Immune response and metabolic regulation are highly integrated. Immune responses during the inflammatory process, if present for some time, can lead to dysmetabolism, which in turn confers more damage on the host [3]. Infection and inflammation cause acute-phase responses and lead to numerous changes in the lipid metabolism. Hyperlipidemia frequently occurs during infectious and inflammatory diseases [4]. Increased plasma triglyceride levels are due to increased very-low-density lipoprotein secretion, which results from accelerated adipose tissue lipolysis, enhanced de novo hepatic fatty acid synthesis, and suppressed fatty acid oxidation [5]. Lipopolysaccharide (LPS) is the main outer membrane component in gram-negative bacteria and is often used to mimic inflammation [6–8]. Ohhira et al. found that LPS induced inflammation and promoted lipid accumulation in mouse livers [9]. Victorov et al. determined that LPS stimulated intracellular lipid accumulation and lipid secretion into the medium in primary cultures of rabbit hepatocytes [10].

Zinc-α2-glycoprotein (ZAG) is an adipokine that was first isolated from plasma [11]. ZAG is a 40-kDa soluble protein, and its crystal structure is similar to that of the class I major histocompatibility complex [12,13]. ZAG is expressed in many tissues, including adipose tissue and liver [14], and its main function is promoting lipid mobilization [15]. Previous research found that ZAG-deficient mice gained more weight than did control mice from ages 7 to 23 weeks [16]. In vitro ZAG stimulated glycerol release from isolated murine adipocytes, and in vivo ZAG caused highly significant decreases in body weight [17]. A previous study showed that ZAG combined with the β-adrenergic receptor (β-AR) to activate the cyclic adenosine monophosphate/protein kinase A (PKA) pathway, eventually accelerating lipolysis under normal conditions [18].

Our previous research revealed that ZAG protein expression was significantly increased after LPS treatment both in serum and white adipose tissue [19]. Similarly, Bao et al. demonstrated that LPS increased ZAG mRNA levels in human adipocytes [20]. However, the role

* Corresponding author.
E-mail address: yangxj@njau.edu.cn (X. Yang).

https://doi.org/10.1016/j.cyto.2019.154742
Received 27 February 2019; Received in revised form 31 May 2019; Accepted 3 June 2019
Available online 28 June 2019
1043-4666/ © 2019 Elsevier Ltd. All rights reserved.

of increased ZAG during inflammation remained largely unknown, and whether ZAG contributed to regulating inflammatory responses and lipid dysmetabolism during inflammation remained unclear. Therefore, we employed LPS-infected ZAG overexpression and knockout mice as models to investigate the function of ZAG during inflammation. We expect that our results will reveal the possible role of ZAG in regulating lipid dysmetabolism during inflammation, clarify the possible underlying mechanisms, and contribute to research on anti-inflammation.

2. Materials and methods

2.1. Ethics statement

Experiments were conducted in accordance with the guidelines of the Animal Ethics Committee of Nanjing Agricultural University, China. Euthanasia and sampling procedures complied with the "Guidelines on Ethical Treatment of Experimental Animals" (2006) No. 398 published by the Ministry of Science and Technology, China, and with the "Regulation Regarding the Management and Treatment of Experimental Animals" (2008) No. 45, published by the Jiangsu Provincial People's Government.

2.2. Animals and experimental design

2.2.1. ZAG overexpression experiment

Six-week-old C57BL/6 male mice (n = 24), weighing 21.67 ± 0.25 g, were obtained from Lingchang BioTech Co., Ltd. (Shanghai, China). Animals were housed in a temperature-controlled room (22 ± 2 °C) with a 12/12 h light-dark cycle. Mice were fed a pellet chow diet and given deionized water ad libitum over a 5-day adaptation period. After this period, mice were randomly assigned to three groups: the control (CON) group (n = 8), the lipopolysaccharide (LPS) group (n = 8), or the LPS and ZAG overexpression (LZO) group (n = 8). The solution was injected via the tail vein.

The CON and ZAG compound solutions were prepared as follows. First, we mixed 20 μg of the pcDNA3.1 (+)-CON plasmid or pcDNA3.1 (+)-ZAG plasmid (PPL50018-2a, Bioworld, USA) and 150 μL OPTI-MEM reduced serum medium (51985042, ThermoFisher, USA) for 10 min. Second, we mixed 20 μL of Lipofectamine 2000 transfection reagent and 150 μL OPTI-MEM reduced serum medium for 10 min. Finally, we mixed these two mixtures for 30 min.

On day 1, the CON and LPS group mice were injected with the CON compound, and the LZO group mice were injected with the ZAG compound. On day 2, we repeated these steps at the same time. One hour after the injection, the CON mice were intraperitoneally injected with equivalent saline. The LPS and LZO mice were intraperitoneally injected with 1 mg/kg *Escherichia coli* 055:B5 LPS (L2880, Sigma-Aldrich). LPS was dissolved in saline and sterilely filtered. Eighteen hours after the intraperitoneal injection, all mice were fasted. After fasting for 6 h, the mice were weighed and sacrificed by exsanguination. The blood was collected via the inferior vena cava into a tube with heparin sodium. After standing on ice for 4 h, the tube was centrifuged, then the whole supernatant was transferred into new tube, and the plasma was stored at −20 °C. The liver was weighed, immediately frozen in liquid nitrogen, and stored at −80 °C until further analysis.

2.2.2. ZAG knockout experiment

Six-week-old normal C57BL/6 female mice (n = 4, weighing 20.73 ± 0.37 g) and six-week-old ZAG systemic knockout C57BL/6 female mice (n = 4, weighing 20.65 ± 0.29 g) were obtained from Nanjing Biomedical Research Institute (NBRI) of Nanjing University, Nanjing, China. The ZAG systemic knockout mice were induced using crispr/cas 9. The knockout fragment was 2968 bp long (AACAATC TCT—GTCAGAAAAG). The two knockout points were separately located on introns 1 and 3. Exons 2 and 3 were completely deleted. The mice were housed in a temperature-controlled room (22 ± 2 °C) with a 12/12 h light-dark cycle. Mice were fed a pellet chow diet and given deionized water ad libitum over a 5-day adaptation period.

In this experiment, the endotoxin (ETX) group (n = 4) and the ETX and ZAG knockout (EZK) group (n = 4) mice were intraperitoneally injected with 1 mg/kg LPS. Eighteen hours after the injection, all mice were fasted. After fasting for 6 h, the mice were weighed and sacrificed by exsanguination. The collection, treatment and conservation of all samples were the same as the above operation.

Table 1
Primer sequences for real-time PCR amplification.

Target genes	Primer sequences
ND6	F: ACAAAGATCACCCAGCTA
	R: GGAGTTATGTTGGAAGGA
IL1α	F: AAGAAGAGACGGCTGAGT
	R: GTGGTGCTGAGATAGTGTT
IL1β	F: CTTCAGGCAGGCAGTATC
	R: CAGCAGGTTATCATCATCATC
IL6	F: GCCTTCTTGGGACTGATGCT
	R: GACAGGTCTGTTGGGAGTGG
IL10	F: CAGAGAAGCATGGCCCAGAA
	R: GCTCCACTGCCTTGCTCTTA
MCP1	F: TCGGAACCAAATGAGATCAGA
	R: TAGCTTCAGATTTACGGGTCA
BAX	F: CCAGGATGCGTCCACCAA
	R: AAAGTAGAAGAGGGCAACCAC
BCL2	F: CTACCGTCGTGACTTCGC
	R: GGGTGACATCTCCCTGTT
BCLXL	F: CAACCCATCCTGGCACCT
	R: ACCGCAGTTCAAACTCATCG
MCL1	F: GGATGGGTTTGTGGAGTT
	R: TGTAGTTTGGTGGCTGGA
PPIA	F: GCAAGACCAGCAAGAAGA
	R: CAGTGAGAGCAGAGATTACA

ND6, NADH dehydrogenase subunit 6; IL1α, interleukin 1α; MCP1, monocyte chemoattractant protein 1; BAX, B cell leukemia/lymphoma 2 associated X; BCL2, B cell leukemia/lymphoma 2; BCLXL, B cell leukemia/lymphoma 2 like 1; MCL1, B cell leukemia/lymphoma 2 family apoptosis regulator; PPIA, peptidylprolyl isomerase A.

Table 2
Apparent and biochemical indexes after ZAG overexpression.

Index	CON	LPS	LZO
Body weight (g)	18.94 ± 0.31	18.95 ± 0.29	19.45 ± 0.40
Liver weight (g)	0.94 ± 0.03	1.07 ± 0.04*	1.03 ± 0.04
Liver index (%)	5.00 ± 0.18	5.64 ± 0.13*	5.29 ± 0.16
Plasma TG (mmol/L)	0.42 ± 0.04	1.64 ± 0.23*	0.84 ± 0.16#
Plasma NEFA (mmol/L)	1.16 ± 0.05	2.27 ± 0.20*	1.62 ± 0.24#

LZO represents the LPS and ZAG overexpression group. Data represent the means ± SEM. Data were considered statistically significant when $P \leq 0.05$.
* $P \leq 0.05$ versus CON.
\# $P \leq 0.05$ versus LPS.

2.3. Plasma biochemical index detection

Plasma triglyceride (TG) and non-esterified fatty acid (NEFA) levels were measured using an automatic biochemical analyzer (7020, HITACHI, Japan). The TG assay kit (999-32991 and 33091) and the NEFA assay kit (999-09801) were purchased from Wako (Japan).

2.4. Liver morphological analysis

Fresh liver samples were prepared for histological examination by fixing in 4% paraformaldehyde-buffered solution, quick-freezing, embedding in optimal cutting temperature compound and sectioning. The samples were then stained with oil red O and observed.

Fresh liver samples were prepared and rapidly fixed with 2.5%

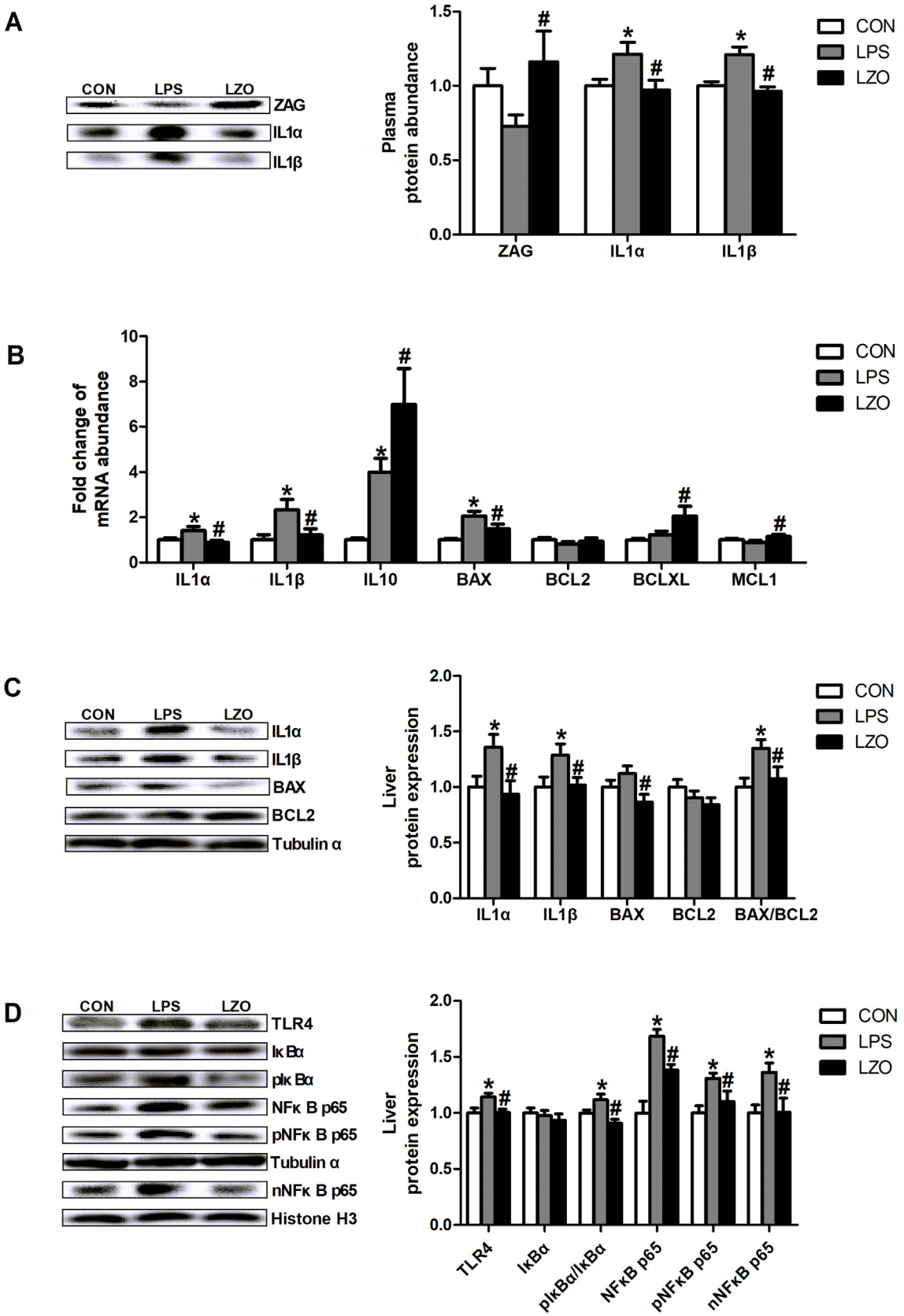

Fig. 1. Plasma protein abundance, hepatic inflammation and apoptosis related gene and protein expressions after ZAG overexpression. Fig. 1A shows the plasma ZAG, IL1α and IL1β protein abundances. The plasma was diluted 10 times, and the protein abundance was measured via western blot. Fig. 1B shows the gene expressions of IL1α, IL1β, IL10, BAX, BCL2, BCLXL and MCL1 in the liver. Gene expression was measured using real-time quantitative PCR. Fig. 1C shows the protein expressions of IL1α, IL1β, BAX, BCL2 and BAX/BCL2 in the liver. Protein expression was measured via western blot. Fig. 1D shows the protein expressions of TLR4, IκBα, phosphorylated IκBα, NFκB p65, phosphorylated NFκB p65 and nuclear NFκB p65. Protein expression was measured via western blot. LZO represents the LPS and ZAG overexpression group. Data represent the means ± SEM. Data were considered statistically significant when $P \leq 0.05$. $^{*}P \leq 0.05$ versus CON; $^{\#}P \leq 0.05$ versus LPS.

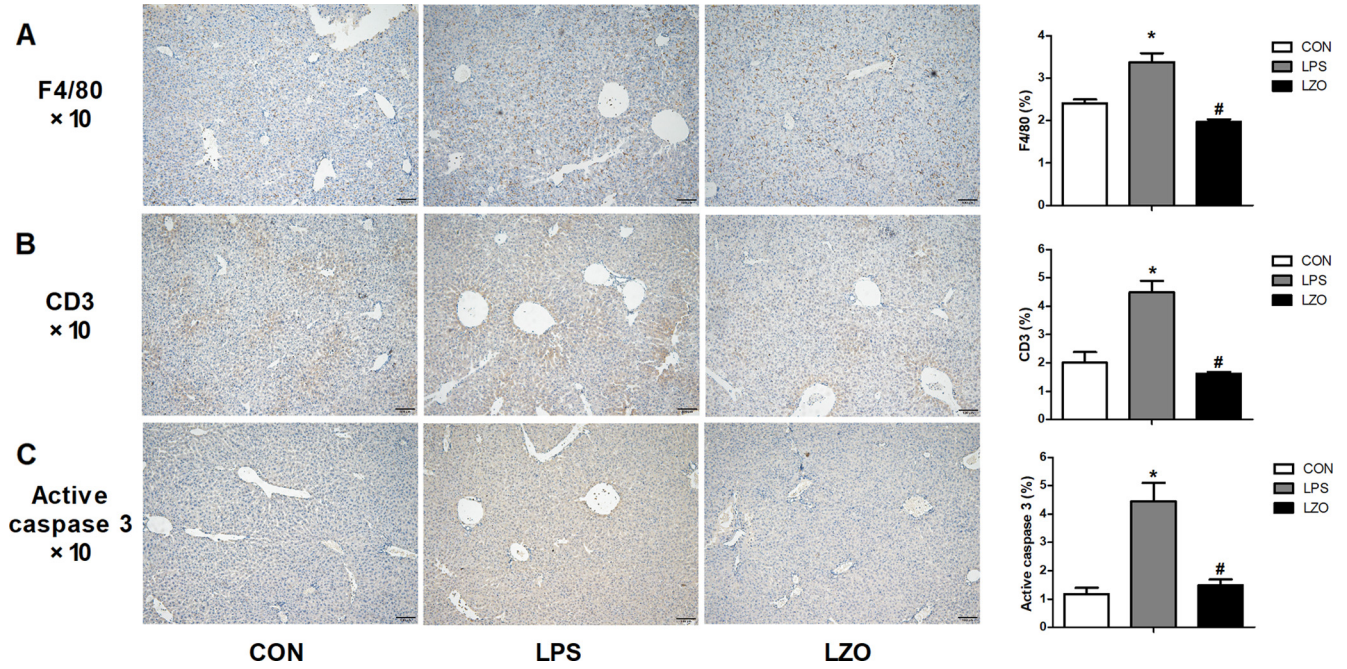

Fig. 2. Liver F4/80, CD3 and active caspase 3 immunohistochemical staining after ZAG overexpression. figure A shows the liver F4/80 immunohistochemical staining and the percentage of immunohistochemical staining. Immunohistochemical staining was analyzed using Image-Pro Plus 6.0. figure B shows the liver CD3 immunohistochemical staining and the percentage of immunohistochemical staining. Immunohistochemical staining was analyzed using Image-Pro Plus 6.0. figure C shows the liver active caspase 3 immunohistochemical staining and the percentage of immunohistochemical staining. Immunohistochemical staining was analyzed using Image-Pro Plus 6.0. LZO represents the LPS and ZAG overexpression group. Data represent the means ± SEM. Data were considered statistically significant when $P \leq 0.05$. $^{*}P \leq 0.05$ versus CON; $^{\#}P \leq 0.05$ versus LPS.

glutaraldehyde, later fixed with 1% osmium tetroxide, and embedded in resin. Next ultrathin sections were cut and stained with uranyl acetate and lead citrate. Finally, hepatic ultrastructure was determined using a transmission electron microscope (Hitachi H-7650, Hitachi Technologies, Tokyo, Japan).

2.5. Liver immunohistochemical analysis

Fresh liver samples were prepared for histological examination by fixing in 4% paraformaldehyde-buffered solution, quick-freezing, embedding in optimal cutting temperature compound, and sectioning.

The tissue was dewaxed in xylene, and antigens repair were performed by boiling the sections in citric acid buffer for 15 min, cooling for 20 min and soaking with 3% hydrogen peroxide for 15 min. For the immunohistochemistry, sections were blocked with 4% goat serum prior to incubation with primary antibody overnight at 4 °C. Finally, each section was incubated with secondary antibody for 30 min prior to colorizing using 3,3′-diaminobenzidine tetrahydrochloride substrate. The primary antibodies used were F4/80 (ab6640, Abcam, UK), CD3 (ab135372, Abcam, UK), and active caspase 3 (#9661, Cell Signaling Technology, USA).

2.6. Hepatic TG content detection

Frozen 50 mg liver samples were prepared, and the hepatic TG content was determined per the instructions with the TG assay kit (E1013), which was purchased from PPLYGEN (Beijing, China).

2.7. Hepatic mitochondrial complex III and V activity detection

Frozen 100 mg liver samples were prepared. Hepatic mitochondrial complex III and V activities were determined per the instructions in the mitochondrial complex III (FHTC-2-Y) and mitochondrial complex V (FHTE-2-Y) activity assay kits purchased from COMIN (Suzhou, China).

2.8. Hepatic mitochondrial DNA copy number detection

Total genomic DNA was extracted from the frozen liver samples. As previously described, the mitochondrial DNA copy number was detected via real-time PCR, with some modifications [21]. Relative mitochondrial DNA levels were determined by calculating the ratio between the mitochondrial NADH dehydrogenase subunit 6 (ND6) and the single-copy nuclear-encoded Peptidylprolyl isomerase A (PPIA) gene (Table 1). The relative mitochondrial DNA copy number was calculated using the $2^{-\Delta\Delta Ct}$ method [22].

2.9. RNA isolation, cDNA synthesis and real-time PCR

Total RNA was extracted from liver samples using Total RNA Isolation Reagent (3101-100, Pufei Biotech, Shanghai, China). The extracted RNA was quantified by using the NanoDrop ND-1000 spectrophotometer (ThermoFisher, USA). The absorption ratios (260/280 nm and 260/230 nm) of all samples were between 1.8 and 2.0, which indicated adequate purity. Some of the RNA samples were used for electrophoresis through a 1.4% agarose-formaldehyde gel to verify the samples' integrity. The RNA (1 μg) was treated with RNase-Free DNase and reverse-transcribed per the manufacturer's instructions (R223-01, Vazyme, Nanjing, China). Diluted cDNA (1:10, vol/vol) was used for real-time PCR, which was detected using the QuantStudio 6 Flex Real-Time PCR System (ThermoFisher, USA). PPIA, which was unaffected by the experimental factors, was chosen as the reference gene. All primers used are shown in Table 1 and were synthesized by Generay (Shanghai, China). The $2^{-\Delta\Delta Ct}$ method was used to analyze the real-time PCR results. Gene mRNA levels were expressed as the fold change relative to the mean value of the CON group.

2.10. Liver preparation, total protein extraction and western blotting

Frozen 50 mg liver samples were minced and homogenized in 500 μL of pre-cooled RIPA buffer containing the protease inhibitor

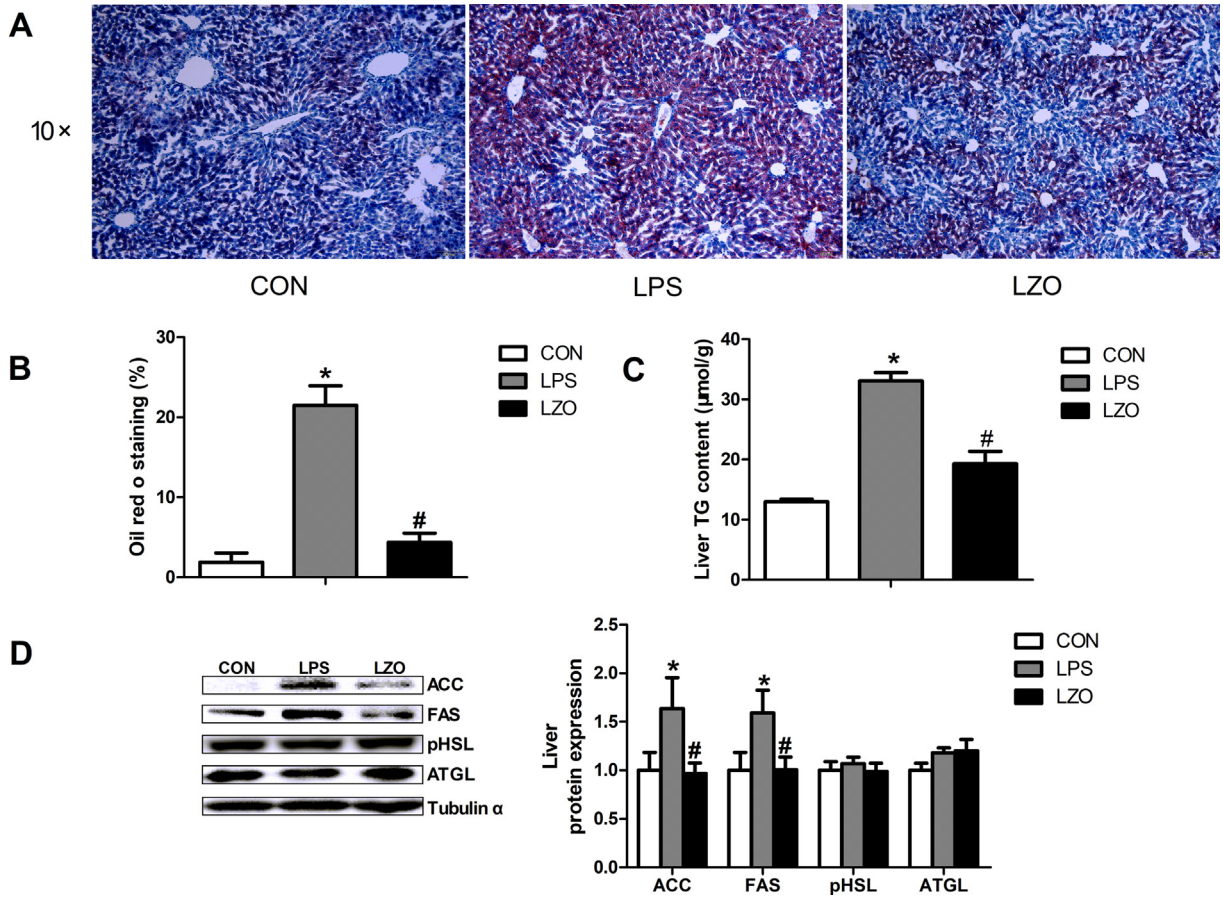

Fig. 3. Liver oil red O staining and lipid metabolism-related protein expression after ZAG overexpression. figure A shows the liver oil red O staining. figure B shows the percentage of oil red O staining. Oil red O staining was analyzed using Image-Pro Plus 6.0. figure C shows the liver TG content. figure D shows the protein expressions of ACC, FAS, phosphorylated HSL and ATGL. The protein expression was measured via western blot. LZO represents the LPS and ZAG overexpression group. Data represent the means ± SEM. Data were considered statistically significant when $P \leq 0.05$. $^{*}P \leq 0.05$ versus CON; $^{\#}P \leq 0.05$ versus LPS.

cocktail of Complete EDTA-free and PhosSTOP (Roche, Penz-berg, Germany). Protein concentration was determined using the BCA Protein Assay kit (Pierce, Rockford, IL, USA). The protein (50 μg) extracted from each sample was then loaded onto 10% sodium dodecyl sulfate-polyacrylamide gel electrophoresis gels, and the separated proteins were transferred onto the nitrocellulose membranes (Bio Trace, Pall Co., USA). After transfer, the membranes were blocked for 2 h at room temperature in blocking buffer, then incubated with the primary antibodies in dilution buffer overnight at 4 °C. After several washes in Tris-buffered-saline with Tween, the membranes were incubated with the secondary antibodies in dilution buffer for 2 h at room temperature. After several washes, the bands were visualized by enhanced chemiluminescence using the LumiGlo substrate (Super Signal West Pico Trial Kit, Pierce, USA), and the signals were recorded using an imaging system (Bio-Rad, USA) and analyzed with Quantity One software (Bio-Rad).

The primary antibodies used were ZAG (ab117275, Abcam, UK), interleukin 1α (IL1α) (WL02541, Wanleibio, China), IL1β (WL02377, Wanleibio, China), B cell leukemia/lymphoma 2 associated X (BAX) (BS2538, Bioworld, USA), B cell leukemia/lymphoma 2 (BCL2) (BS1511, Bioworld, USA), TLR4 (WL00196, Wanleibio, China), nuclear factor of kappa light polypeptide gene enhancer in B-cells inhibitor, alpha (IκBα) (WL00148, Wanleibio, China), phosphorylated IκBα (WL02495, Wanleibio, China), NFκB p65 (WL01980, Wanleibio, China), phosphorylated NFκB p65 (pNFκB p65) (WL02169, Wanleibio, China), acetyl-CoA carboxylase 1 (ACC) (BS1377, Bioworld, USA), fatty acid synthase (FAS) (BS6050, Bioworld, USA), phosphorylated hormone-sensitive lipase (pHSL) (BS4234, Bioworld, USA), adipose triglyceride lipase (ATGL) (BS7989, Bioworld, USA), cytochrome *c* oxidase subunit 1 (COX1) (BS1636, Bioworld, USA), uncoupling protein 3 (UCP3) (BS2849, Bioworld, USA), β3-AR (M-20, Santa Cruz, USA), PKA (BS1576, Bioworld, USA), cyclic adenosine monophosphate-response element binding protein (CREB) (BS1077, Bioworld, USA), phosphorylated CREB (BS4053, Bioworld, USA), histone h3 (ab1791, Abcam, UK), and tubulin α (BS1699, Bioworld, USA). The secondary antibodies were goat anti-rabbit horseradish peroxidase antibody (BS13278, Bioworld, USA) and rabbit anti-goat horseradish peroxidase antibody (BS30503, Bioworld, USA).

2.11. Co-immunoprecipitation

Five hundred microliters of 50% protein A/G plus agarose (sc-2003, Santa Cruz, CA, USA) was prepared using pre-cooled RIPA buffer without the protease inhibitor. Liver protein was extracted, and the protein concentration was quantified via western blot. Each protein sample (500 μg, 5 μg/μL) was mixed with 20 μL of 50% protein A/G plus agarose beads and incubated for 2 h at 4 °C on a rotary shaker. The mixture was centrifuged for 1 min at 4 °C at 10000 rpm. The supernatant was transferred to a new tube, and 30 μL was left for input. The remaining supernatant was mixed with CBP antibody (1.5 μg, ab50702, Abcam, UK). The mixture was incubated overnight at 4 °C on a rotary shaker. Next, 20 μL of 50% protein A/G plus agarose beads were added and incubated overnight at 4 °C on a rotary shaker. The mixture was centrifuged for 1 min at 4 °C at 10000 rpm. The supernatant was then removed, and the beads were mixed with 20 μL of 6 × sodium dodecyl sulfate loading buffer and denatured by boiling for 5 min. The CREB

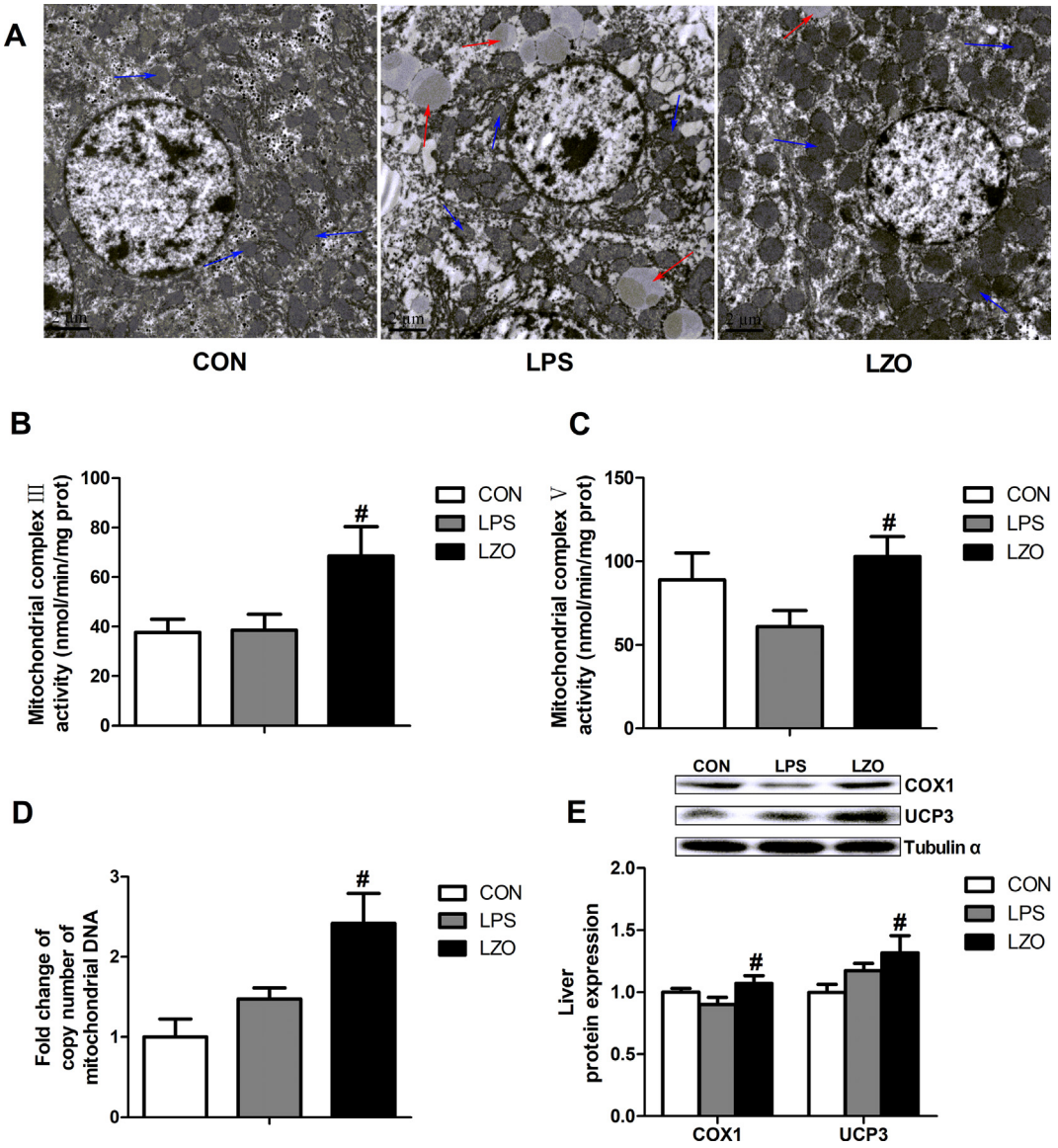

Fig. 4. Liver transmission electron microscopy and ultramicrotomy, mitochondrial complex III and V activity, mitochondrial DNA copy number and energy metabolism-related protein expression. figure A shows the liver transmission electron microscopy and ultramicrotomy. The red arrows point to the lipid droplets and the blue arrows point to the mitochondria. figure B shows the hepatic mitochondrial complex III activity. figure C shows the hepatic mitochondrial complex V activities. figure D shows the hepatic mitochondrial DNA copy numbers. The mitochondrial DNA copy number was measured via real-time quantitative PCR. figure E shows the protein expressions of COX1 and UCP3. Protein expression was measured via western blot. LZO represents the LPS and ZAG overexpression group. Data represent the means ± SEM. Data were considered statistically significant when $P \leq 0.05$. $^{*}P \leq 0.05$ versus CON; $^{\#}P \leq 0.05$ versus LPS.

and NFκB combined with CBP was detected via western blot.

2.12. Statistical analysis

All statistical analyses were performed using SPSS 18.0 for Windows (IBM Corp., Armonk, NY, USA). All data are expressed as the mean ± SEM. One-way ANOVA was used to identify significant differences in the ZAG overexpression experiment, and t-tests were used to identify significant differences in the ZAG knockout experiment. The significance level was set at $P \leq 0.05$ for all analyses.

3. Results

3.1. Apparent and biochemical indexes after ZAG overexpression

LPS treatment increased the liver weight and index; ZAG overexpression did not affect on these values compared with the LPS group. LPS treatment increased the plasma TG and NEFA content, while ZAG overexpression decreased these values (Table 2).

3.2. Inflammation and apoptosis changes after ZAG overexpression

ZAG protein levels in the plasma increased after ZAG overexpression compared with those of the LPS group (Fig. 1A). LPS treatment increased the plasma IL1α and IL1β protein abundances, which were decreased by ZAG overexpression. LPS treatment increased the IL1α, IL1β, IL10 and BAX gene expressions; ZAG overexpression decreased the IL1α, IL1β and BAX gene expressions. ZAG overexpression increased the IL10, BCLXL and MCL1 gene expressions compared with those of the LPS group (Fig. 1B). LPS treatment increased the protein levels of IL1α and IL1β; ZAG overexpression decreased these values compared with those of the LPS group. LPS treatment increased BAX/BCL2, while ZAG overexpression decreased this ratio (Fig. 1C). LPS treatment increased TLR4, phosphorylated IκBα, NFκB p65,

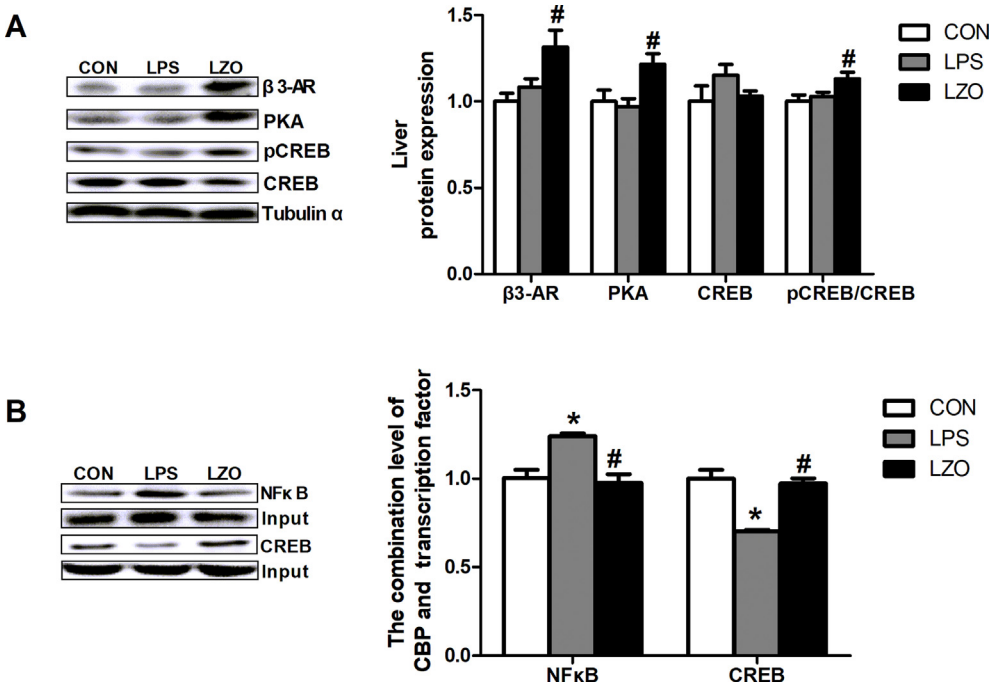

Fig. 5. Liver β3-AR/PKA/CREB pathway related protein expression and protein abundances of CREB and NFκB p65, which combined with CBP after ZAG overexpression. figure A shows the protein expressions of β3-AR, PKA, CREB and phosphorylated CREB after ZAG overexpression. The protein expression was measured via western blot. figure B shows the protein abundances of CREB and NFκB p65, which combined with CBP. The degree of combination was measured via co-immunoprecipitation. The liver protein was incubated with protein A/G plus agarose beads and CBP antibody, then the combined CREB and combined NFκB p65 were measured via western blot. LZO represents the LPS and ZAG overexpression group. Data represent the means ± SEM. Data were considered statistically significant when $P \leq 0.05$. $^{*}P \leq 0.05$ versus CON; $^{\#}P \leq 0.05$ versus LPS.

Table 3
Apparent and biochemical indexes after ZAG knockout.

Index	ETX	EZK
Body weight (g)	18.33 ± 0.32	18.29 ± 0.36
Liver weight (g)	0.95 ± 0.03	0.88 ± 0.03
Liver index (%)	5.19 ± 0.10	4.79 ± 0.11*
Plasma TG (mmol/L)	1.66 ± 0.51	3.68 ± 0.71 (P = 0.08)
Plasma NEFA (mmol/L)	2.06 ± 0.21	2.70 ± 0.17 (P = 0.08)

EZK represents the ETX and ZAG knockout group. Data represent the means ± SEM. Data were considered statistically significant when $P \leq 0.05$.
* $P \leq 0.05$ versus ETX.

phosphorylated NFκB p65 and nuclear NFκB p65 levels; ZAG overexpression decreased these levels compared with the LPS group (Fig. 1D).

LPS treatment increased the macrophage surface marker F4/80 protein abundance in the liver, while ZAG overexpression decreased it compared with the LPS group (Fig. 2A). LPS treatment increased T cell surface marker CD3 protein abundance in the liver, while ZAG overexpression decreased it compared with the LPS group (Fig. 2B). LPS treatment increased hepatic active caspase 3 protein abundance, whereas ZAG overexpression decreased it compared with the LPS group (Fig. 2C).

3.3. Lipid metabolism change after ZAG overexpression

Oil red O staining revealed that LPS treatment increased the hepatic lipid content, while ZAG overexpression decreased it (Fig. 3A and 3B). ZAG overexpression also alleviated the high LPS-induced hepatic TG content (Fig. 3C). LPS treatment increased ACC and FAS protein levels, while ZAG overexpression reduced them compared with the LPS group (Fig. 3D). pHSL and ATGL protein levels were unchanged in both the LPS and LZO groups.

3.4. Energy metabolism changes after ZAG overexpression

Lipid droplets increased in number in the LPS group (Fig. 4A). After ZAG overexpression, the lipid droplets decreased, and the mitochondria became larger and deepened in color. ZAG overexpression increased the mitochondrial complex III and V activities compared with those in the LPS group (Fig. 4B and 4C). Mitochondrial DNA copy number also increased after ZAG overexpression compared with the LPS group (Fig. 4D). ZAG overexpression increased the COX1 and UCP3 protein levels compared with the LPS group (Fig. 4E).

3.5. β3-AR/PKA/CREB pathway change after ZAG overexpression

ZAG works primarily through the β3-AR/PKA pathway. Activated PKA can phosphorylate CREB to influence inflammation. Therefore, β3-AR, PKA, CREB and phosphorylated CREB protein levels were detected. ZAG overexpression increased β3-AR, PKA and phosphorylated CREB protein levels compared with the LPS group (Fig. 5A). When phosphorylated NFκB translocated into the nucleus, it combined with CBP to form the NFκB-CBP complex, eventually inducing inflammation. However, phosphorylated CREB can combine with CBP to form the CREB-CBP complex, eventually suppressing inflammation. Therefore, the combined degree of NFκB and CBP and the combined degree of CREB and CBP were detected. LPS treatment suppressed the combination of CREB and CBP, and promoted the combination of NFκB and CBP (Fig. 5B). ZAG overexpression promoted the combination of CREB and CBP and suppressed the combination of NFκB and CBP.

3.6. Apparent and biochemical indexes after ZAG knockout

The above results suggest that ZAG overexpression alleviated LPS-induced inflammation and hyperlipemia. ZAG knockout mice were used to confirm the function of ZAG during inflammation. ZAG knockout decreased the liver index compared with the ETX group, although the body and liver weights remained unchanged (Table 3). Plasma TG (P = 0.08) and NEFA (P = 0.08) had a trend to increase in the EZK group compared with the ETX group.

3.7. Inflammation and metabolic changes after ZAG knockout

Plasma ZAG protein disappeared after ZAG knockout. ZAG knockout increased the plasma IL1α and IL1β protein abundances (Fig. 6A). After ZAG knockout, gene expression of hepatic IL1α, IL1β, IL6 and MCP1 increased (Fig. 6B). After ZAG knockout, ACC and FAS protein levels

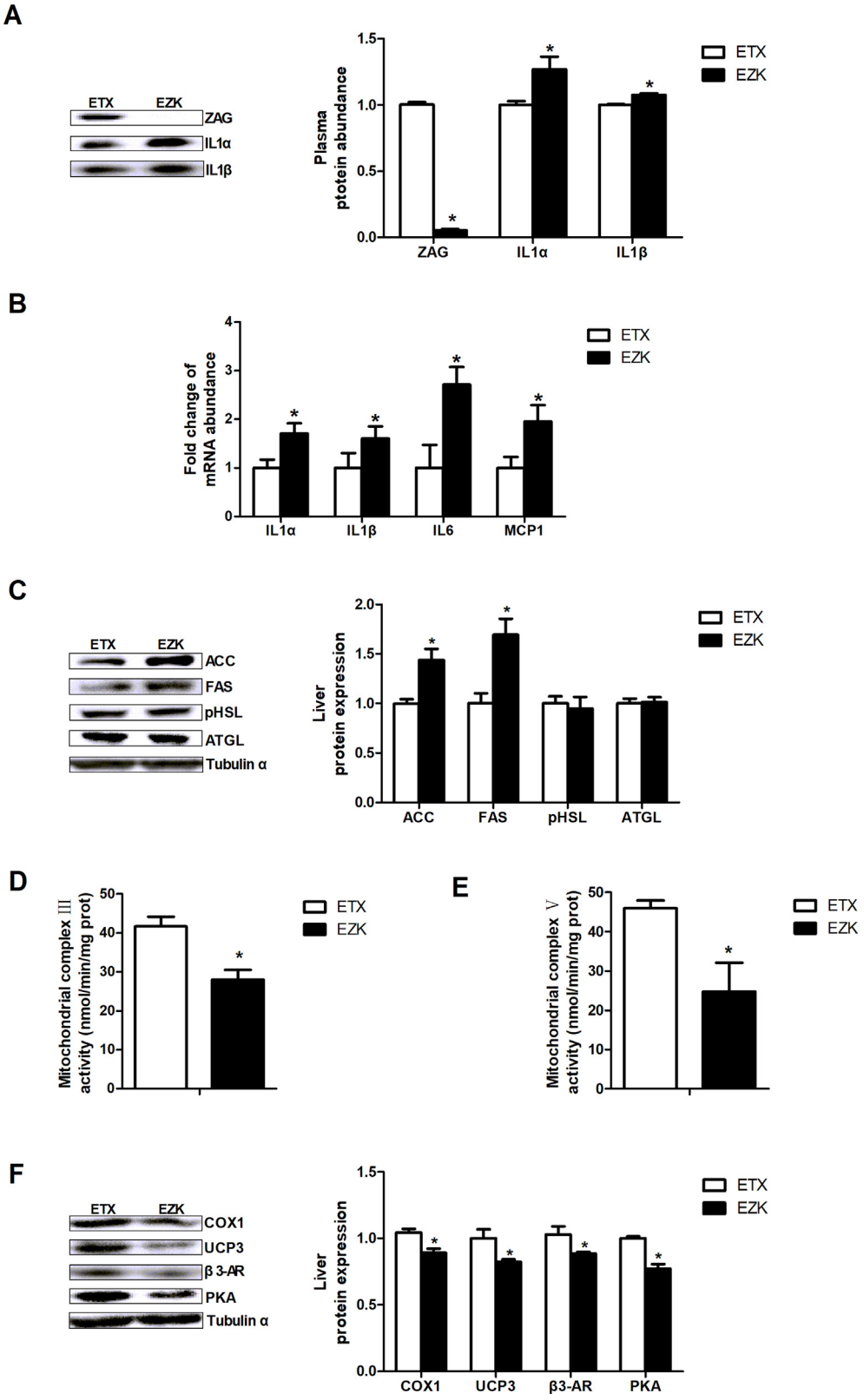

Fig. 6. Inflammation, lipid metabolism, energy metabolism and β3-AR/PKA pathway related gene and protein expression and enzyme activity after ZAG knockout. figure A shows the plasma ZAG, IL1α and IL1β protein abundances. The plasma was diluted 10 times, and the protein abundance was measured via western blot. figure B shows the gene expressions of IL1α, IL1β, IL6 and MCP1 in the liver. The gene expression was measured using real-time quantitative PCR. figure C shows the protein expressions of ACC, FAS, phosphorylated HSL and ATGL. Protein expression was measured via western blot. figure D shows the hepatic mitochondrial complex III activity. figure E shows the hepatic mitochondrial complex V activity. figure F shows the protein expressions of COX1, UCP3, β3-AR and PKA. Protein expression was measured via western blot. EZK represents the ETX and ZAG knockout group. Data represent the means ± SEM. Data were considered statistically significant when $P \leq 0.05$. $^{*}P \leq 0.05$ versus ETX.

increased compared with those in the ETX group. However, pHSL and ATGL remained unchanged (Fig. 6C). ZAG knockout decreased the mitochondrial complex III and V activities (Fig. 6D and 6E) and the COX1 and UCP3 protein levels compared with those in the ETX group (Fig. 6F). ZAG overexpression decreased the β3-AR and PKA protein levels compared with the ETX group.

4. Discussion

Activated inflammatory responses lead to lipid dysmetabolism, which can immeasurably harm the body. ZAG, a newly discovered adipokine, plays a role in lipolysis [17]. However, few researchers have studied ZAG's action on inflammatory responses and substance

metabolism during inflammation. Therefore, we used an LPS challenge to mimic inflammation and used ZAG overexpression and knockout mice to explore the possible role of ZAG in the inflammatory state. The results showed that ZAG overexpression obviously alleviated the severe LPS-induced inflammatory responses. ZAG overexpression significantly decreased the plasma lipid content, which was increased by LPS treatment. After ZAG knockout, the LPS-induced inflammation and hyperlipidemia worsened.

Until now, no research has studied the effects of ZAG on inflammatory responses. Therefore, this research was the first to explore its newly discovered function. We found that plasma proinflammatory factors (IL1α and IL1β) increased after LPS treatment and decreased after ZAG overexpression. ZAG exerted a similar effect on proinflammatory factor production in the liver. ZAG overexpression increased gene expression of the anti-inflammatory factor (IL10). F4/80 is macrophage surface marker, and CD3 is T cell surface marker. Immunohistochemical analysis found that ZAG overexpression decreased these two markers compared with the LPS group, suggesting that ZAG overexpression decreased LPS-induced immune cell infiltration. Thus, ZAG played an important role in anti-inflammation both in the whole body and in local tissues. Severe inflammation often results in apoptosis [23]. The present study demonstrated that LPS induced hepatic cell apoptosis, while ZAG overexpression decreased the proapoptotic cytokine, BAX/BCL2, and increased the antiapoptotic cytokines, BCLXL and MCL1. Immunohistochemical analysis suggested that ZAG overexpression decreased active caspase 3 compared with the LPS group. The inhibitory effect of ZAG on apoptosis was mainly due to decreased inflammatory factors. Because ZAG is involved in repressing inflammation, the specific mechanism of this repression should be explored. The TLR4/NFκB pathway is the main pathway during inflammation [24–26]. Our results revealed that LPS increased the protein expressions of TLR4, phosphorylated IκBα, phosphorylated NFκB p65 and total NFκB p65 and promoted nuclear translocation of NFκB p65. ZAG overexpression decreased the expressions of these proteins and suppressed NFκB p65 translocation to the nucleus. Therefore, ZAG inhibited the LPS-induced TLR4/NFκB inflammatory pathway activation, suppressed proinflammatory factor expression and promoted anti-inflammatory factor expression.

A previous study showed that LPS stimulates intracellular lipid accumulation [27], which is consistent with our results. The present results showed that ZAG overexpression reduced hepatic TG content, although we did not find that ZAG overexpression promoted lipolysis (pHSL and ATGL) in the liver. Regarding corresponding mechanisms, two lipogenesis-related key enzymes, ACC and FAS, decreased after ZAG overexpression. ZAG reduces body weight primarily by reducing body fat via promoting lipolysis in adipose tissue [28]; however, many reports show the action of ZAG on lipogenesis. Gong et al. found that FAS mRNA expression was decreased in the liver in ZAG overexpression mice [29]. Xiao et al. found that ZAG overexpression inhibited lipogenesis in hepatocytes, while ZAG interference accelerated them [30]. The present research revealed no direct correlation between ZAG and lipogenesis during inflammation; thus, the most probable explanation is that the repressive effects of ZAG on lipogenesis resulted from the reduced inflammation.

Mitochondrial morphological analysis suggested that ZAG overexpression enhanced mitochondrial function. Mitochondrial DNA (mtDNA) regulates mitochondrial oxidative phosphorylation, and mtDNA is recognized in multiple copies per mitochondrion [31]. In our results, increased hepatic mtDNA copy number after ZAG overexpression indicated that ZAG accelerated mitochondrial biogenesis and enhanced mitochondrial function. Enzyme activities of mitochondrial complexes III and V showed the same changes as the mtDNA. Regarding molecular levels, ZAG overexpression increased COX1 and UCP3 protein levels. Recent research on the effects of ZAG on energy metabolism have focused on UCP in adipose tissue and muscle. Sanders et al. confirmed that ZAG can directly induce UCP expression in brown adipose tissue and skeletal muscle [32]. Russell et al. confirmed that after ZAG treatment in ob/ob mice for 5 d, UCP1 and UCP3 protein expression increased in the brown adipose tissue, and UCP3 increased in the gastrocnemius muscle [33]. These results indicate that ZAG overexpression enhanced mitochondrial function and energy metabolism; thus, the body consumed more NEFA in the plasma and liver.

Several studies demonstrated that when NFκB was activated and translocated into the nucleus, it interacted with the transcriptional coactivator CREB-binding protein (CBP), further combining to the promoter of inflammatory cytokines and then promoting transcription of proinflammatory factors and inhibiting transcription of antiinflammatory factors [34,35]. ZAG may work through the β3-AR/PKA pathway [36]. Several researchers found that PKA induced CREB phosphorylation, and phosphorylated CREB promoted CREB binding to CBP to form the CREB-CBP complex, which could suppress formation of the NFκB-CBP complex and reduce inflammation [37–39]. In our experiment, ZAG overexpression increased β3-AR and PKA expression, induced CREB phosphorylation, promoted CREB-CBP complex formation, and suppressed NFκB-CBP complex formation, eventually alleviating inflammation.

To further confirm the effects of ZAG on inflammatory responses and substance metabolism during inflammation, we analyzed the corresponding changes in ZAG knockout mice. After ZAG knockout, inflammatory responses intensified, lipogenesis heightened, mitochondrial function decreased, and the β3-AR/PKA pathway signal was decreased. These results in the knockout mice were consistent with ZAG function in the overexpression mice.

In summary, ZAG alleviated lipid metabolism disorders by weakening inflammatory responses. The β3-AR/PKA/CREB pathway mediated the effects of ZAG on inflammation. These results will provide new insight for anti-inflammation research.

Funding

This study was supported by the National Natural Science Foundation of China (31572482 and 31772696), and the Priority Academic Program Development of Jiangsu Higher Education Institutions.

Declaration of Competing Interest

None.

References

[1] P. Rajendran, Y.F. Chen, Y.F. Chen, L.C. Chung, S. Tamilselvi, C.Y. Shen, C.H. Day, R.J. Chen, V.P. Viswanadha, W.W. Kuo, C.Y. Huang, The multifaceted link between inflammation and human diseases, J. Cell. Physiol. 233 (9) (2018) 6458–6471.
[2] J.A. Jiminez, T.C. Uwiera, G. Douglas Inglis, R.R. Uwiera, Animal models to study acute and chronic intestinal inflammation in mammals, Gut Pathogens 7 (2015) 29.
[3] R.M. Loftus, D.K. Finlay, Immunometabolism: cellular metabolism turns immune regulator, J. Biol. Chem. 291 (1) (2016) 1–10.
[4] R. Cheluvappa, G.M. Denning, G.W. Lau, M.C. Grimm, S.N. Hilmer, D.G. Le Couteur, Pseudomonas aeruginosa and the hyperlipidaemia of sepsis, Pathology 41 (7) (2009) 615–621.
[5] W. Khovidhunkit, M.S. Kim, R.A. Memon, J.K. Shigenaga, A.H. Moser, K.R. Feingold, C. Grunfeld, Effects of infection and inflammation on lipid and lipoprotein metabolism: mechanisms and consequences to the host, J. Lipid Res. 45 (7) (2004) 1169–1196.
[6] A. Tagashira, K. Nishi, T. Sugahara, Lysozyme from hen egg white ameliorates lipopolysaccharide-induced systemic inflammation in mice, Cytotechnology (2019).
[7] D. Wang, Q. Gao, G. Zhao, Z. Kan, X. Wang, H. Wang, J. Huang, T. Wang, F. Qian, C.T. Ho, Y. Wang, Protective effect and mechanism of theanine on lipopolysaccharide-induced inflammation and acute liver injury in mice, J. Agric. Food. Chem. 66 (29) (2018) 7674–7683.
[8] Z. Guo, Z. Li, Y. Deng, S.L. Chen, Photoacoustic microscopy for evaluating a lipopolysaccharide-induced inflammation model in mice, J. Biophoton. (2018) e201800251.
[9] M. Ohhira, W. Motomura, M. Fukuda, T. Yoshizaki, N. Takahashi, S. Tanno, N. Wakamiya, Y. Kohgo, S. Kumei, T. Okumura, Lipopolysaccharide induces adipose differentiation-related protein expression and lipid accumulation in the liver through inhibition of fatty acid oxidation in mice, J. Gastroenterol. 42 (12) (2007)

969–978.
[10] A.V. Victorov, E.M. Gladkaya, D.K. Novikov, V.A. Kosykh, V.A. Yurkiv, Lipopolysaccharide toxin can directly stimulate the intracellular accumulation of lipids and their secretion into medium in the primary culture of rabbit hepatocytes, FEBS Lett. 256 (1–2) (1989) 155–158.
[11] W. Burgi, K. Schmid, Preparation and properties of Zn-alpha 2-glycoprotein of normal human plasma, J. Biol. Chem. 236 (1961) 1066–1074.
[12] M.I. Hassan, V. Kumar, T.P. Singh, S. Yadav, Purification and characterization of zinc alpha2-glycoprotein-prolactin inducible protein complex from human seminal plasma, J. Sep. Sci. 31 (12) (2008) 2318–2324.
[13] H. Zahid, L. Miah, A.M. Lau, L. Brochard, D. Hati, T.T. Bui, A.F. Drake, J. Gor, S.J. Perkins, L.C. McDermott, Zinc-induced oligomerization of zinc alpha2 glycoprotein reveals multiple fatty acid-binding sites, Biochem. J. 473 (1) (2016) 43–54.
[14] T. Tada, I. Ohkubo, M. Niwa, M. Sasaki, H. Tateyama, T. Eimoto, Immunohistochemical localization of Zn-alpha 2-glycoprotein in normal human tissues, J. Histochem. Cytochem.: Off. J. Histochem. Soc. 39 (9) (1991) 1221–1226.
[15] C. Bing, T. Mracek, D. Gao, P. Trayhurn, Zinc-alpha2-glycoprotein: an adipokine modulator of body fat mass? Int. J. Obesity 34 (11) (2010) 1559–1565.
[16] V. Rolli, M. Radosavljevic, V. Astier, C. Macquin, I. Castan-Laurell, V. Visentin, C. Guigne, C. Carpene, P. Valet, S. Gilfillan, S. Bahram, Lipolysis is altered in MHC class I zinc-alpha(2)-glycoprotein deficient mice, FEBS Lett. 581 (3) (2007) 394–400.
[17] S.T. Russell, T.P. Zimmerman, B.A. Domin, M.J. Tisdale, Induction of lipolysis in vitro and loss of body fat in vivo by zinc-alpha2-glycoprotein, Biochimica et biophysica acta 1636 (1) (2004) 59–68.
[18] C. Bing, Y. Bao, J. Jenkins, P. Sanders, M. Manieri, S. Cinti, M.J. Tisdale, P. Trayhurn, Zinc-alpha2-glycoprotein, a lipid mobilizing factor, is expressed in adipocytes and is up-regulated in mice with cancer cachexia, PNAS 101 (8) (2004) 2500–2505.
[19] J. Guo, Z. Liu, H. Sun, Y. Huang, E. Albrecht, R. Zhao, X. Yang, Lipopolysaccharide challenge significantly influences lipid metabolism and proteome of white adipose tissue in growing pigs, Lipids Health Dis. 14 (2015) 68.
[20] Y. Bao, C. Bing, L. Hunter, J.R. Jenkins, M. Wabitsch, P. Trayhurn, Zinc-alpha2-glycoprotein, a lipid mobilizing factor, is expressed and secreted by human (SGBS) adipocytes, FEBS Lett. 579 (1) (2005) 41–47.
[21] J. Piechota, R. Szczesny, K. Wolanin, A. Chlebowski, E. Bartnik, Nuclear and mitochondrial genome responses in HeLa cells treated with inhibitors of mitochondrial DNA expression, Acta biochimica Polonica 53 (3) (2006) 485–495.
[22] K.J. Livak, T.D. Schmittgen, Analysis of relative gene expression data using real-time quantitative PCR and the 2(-Delta Delta C(T)) method, Methods 25 (4) (2001) 402–408.
[23] J. Zhong, J.V. Deaciuc, R. Burikhanov, W.J.S. de Villiers, Lipopolysaccharide-induced liver apoptosis is increased in interleukin-10 knockout mice, BBA-Mol Basis Dis 1762 (4) (2006) 468–477.
[24] M.P. Jiang, C. Xu, Y.W. Guo, Q.J. Luo, L. Li, H.L. Liu, J. Jiang, H.X. Chen, X.Q. Wei, beta-arrestin 2 attenuates lipopolysaccharide-induced liver injury via inhibition of TLR4/NF-kappa B signaling pathway-mediated inflammation in mice, World J. Gastroenterol. 24 (2) (2018) 216–225.
[25] J. Guo, L.H. Zheng, L. Chen, N. Luo, W.H. Yang, X.Y. Qu, M.M. Liu, Z.P. Cheng, Lipopolysaccharide activated TLR4/NF-kappa B signaling pathway of fibroblasts from uterine fibroids, Int. J. Clin. Exp. Path. 8 (9) (2015) 10014–10025.
[26] J. Wang, Y.F. Si, C. Wu, L. Sun, Y.D. Ma, A.L. Ge, B.M. Li, Lipopolysaccharide promotes lipid accumulation in human adventitial fibroblasts via TLR4-NF-kappa B pathway, Lipids Health Dis. 11 (2012).
[27] X.Y. Li, C. Wang, X.R. Xiang, F.C. Chen, C.M. Yang, J. Wu, Porphyromonas gingivalis lipopolysaccharide increases lipid accumulation by affecting CD36 and ATP-binding cassette transporter A1 in macrophages, Oncol. Rep. 30 (3) (2013) 1329–1336.
[28] M.J. Tisdale, Zinc-alpha2-glycoprotein in cachexia and obesity, Curr. Opin. Support. Palliative Care 3 (4) (2009) 288–293.
[29] F.Y. Gong, J.Y. Deng, H.J. Zhu, H. Pan, L.J. Wang, H.B. Yang, Fatty acid synthase and hormone-sensitive lipase expression in liver are involved in zinc-alpha2-glycoprotein-induced body fat loss in obese mice, Chinese Med. Sci. J. = Chung-kuo i hsueh k'o hsueh tsa chih 25 (3) (2010) 169–175.
[30] X. Xiao, H. Li, X. Qi, Y. Wang, C. Xu, G. Liu, G. Wen, J. Liu, Zinc alpha2 glycoprotein alleviates palmitic acid-induced intracellular lipid accumulation in hepatocytes, Mol. Cell. Endocrinol. 439 (2017) 155–164.
[31] M. Falkenberg, N.G. Larsson, C.M. Gustafsson, DNA replication and transcription in mammalian mitochondria, Annu. Rev. Biochem. 76 (2007) 679–699.
[32] P.M. Sanders, M.J. Tisdale, Effect of zinc-alpha2-glycoprotein (ZAG) on expression of uncoupling proteins in skeletal muscle and adipose tissue, Cancer Lett. 212 (1) (2004) 71–81.
[33] S.T. Russell, M.J. Tisdale, Antidiabetic properties of zinc-alpha2-glycoprotein in ob/ob mice, Endocrinology 151 (3) (2010) 948–957.
[34] P.A. Baeuerle, T. Henkel, Function and activation of NF-kappa B in the immune system, Annu. Rev. Immunol. 12 (1994) 141–179.
[35] M. Karin, Y. Ben-Neriah, Phosphorylation meets ubiquitination: the control of NF-[kappa]B activity, Annu. Rev. Immunol. 18 (2000) 621–663.
[36] S.T. Russell, M.J. Tisdale, Role of beta-adrenergic receptors in the anti-obesity and anti-diabetic effects of zinc-alpha2-glycoprotien (ZAG), Biochimica et biophysica acta 1821 (4) (2012) 590–599.
[37] R. Medzhitov, T. Horng, Transcriptional control of the inflammatory response, Nat. Rev. Immunol. 9 (10) (2009) 692–703.
[38] M. Ghosh, Y. Xu, D.D. Pearse, Cyclic AMP is a key regulator of M1 to M2a phenotypic conversion of microglia in the presence of Th2 cytokines, J. Neuroinflammation 13 (2016) 9.
[39] T. Park, H. Chen, K. Kevala, J.W. Lee, H.Y. Kim, N-Docosahexaenoylethanolamine ameliorates LPS-induced neuroinflammation via cAMP/PKA-dependent signaling, J. Neuroinflammation 13 (1) (2016) 284.